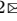



# Reliable Multimodality Eye Disease Screening via Mixture of Student’s $t$ Distributions

Ke Zou<sup>1,2,\*</sup>, Tian Lin<sup>3,4,\*</sup>, Xuedong Yuan<sup>1,2</sup>, Haoyu Chen<sup>3,4</sup>,  
Xiaojing Shen<sup>1,5</sup>, Meng Wang<sup>6</sup>, Huazhu Fu<sup>6</sup>

<sup>1</sup> National Key Laboratory of Fundamental Science on Synthetic Vision, Sichuan University, Sichuan, China

<sup>2</sup> College of Computer Science, Sichuan University, Sichuan, China

<sup>3</sup> Joint Shantou International Eye Center, Shantou University and the Chinese University of Hong Kong, Guangdong, China

<sup>4</sup> Medical College, Shantou University, Guangdong, China

<sup>5</sup> College of Mathematics, Sichuan University, Sichuan, China

<sup>6</sup> Institute of High Performance Computing, A\*STAR, Singapore  
yxd@scu.edu.cn; drchenhaoyu@gmail.com

**Abstract.** Multimodality eye disease screening is crucial in ophthalmology as it integrates information from diverse sources to complement their respective performances. However, the existing methods are weak in assessing the reliability of each unimodality, and directly fusing an unreliable modality may cause screening errors. To address this issue, we introduce a novel multimodality evidential fusion pipeline for eye disease screening, EyeMoSt, which provides a measure of confidence for unimodality and elegantly integrates the multimodality information from a multi-distribution fusion perspective. Specifically, our model estimates both local uncertainty for unimodality and global uncertainty for the fusion modality to produce reliable classification results. More importantly, the proposed mixture of Student’s  $t$  distributions adaptively integrates different modalities to endow the model with heavy-tailed properties, increasing robustness and reliability. Our experimental findings on both public and in-house datasets show that our model is more reliable than current methods. Additionally, EyeMoSt has the potential ability to serve as a data quality discriminator, enabling reliable decision-making for multimodality eye disease screening.

**Keywords:** Multimodality · uncertainty estimation · eye disease.

## 1 Introduction

Retinal fundus images and Optical Coherence Tomography (OCT) are common 2D and 3D imaging techniques used for eye disease screening. Multimodality learning usually provides more complementary information than unimodality learning [3, 4, 31]. This motivates researchers to integrate multiple modalities to

---

\* denotes equal contribution.

improve the performance of eye disease screening. Current multimodality learning methods can be roughly classified into early, intermediate, and late fusion, depending on the fusion stage [2]. For multimodality ophthalmic image learning, recent works have mainly focused on the early fusion [10, 15, 23] and intermediate fusion stages [3, 4, 16, 27]. Early fusion-based approaches integrate multiple modalities directly at the data level, usually by concatenating the raw or preprocessed multimodality data. Hua *et al.* [10] combined preprocessed fundus images and wide-field swept-source optical coherence tomography angiography at the early stage and then extracted representational features for diabetic retinopathy recognition. Intermediate fusion strategies allow multiple modalities to be fused at different intermediate layers of the neural networks. He *et al.* [9] extracted different modality features with convolutional block attention module [28] and modality-specific attention mechanisms, then concatenated them to realize the multimodality fusion for retinal image classification. However, few studies have explored multimodality eye disease screening at the late fusion stage. Furthermore, the above methods do not adequately assess the reliability of each unimodality, and may directly fuse an unreliable modality with others. This could lead to screening errors and be challenging for real-world clinical safety deployment. To achieve this goal, we propose a reliable framework for the multimodality eye disease screening, which provides a confidence (uncertainty) measure for each unimodality and adaptively fuses multimodality predictions in principle.

Uncertainty estimation is an effective way to provide a measure of reliability for ambiguous network predictions. The current uncertainty estimation methods mainly include Bayesian neural networks, deep ensemble methods, and deterministic-based methods. Bayesian neural networks [18, 21, 22] learn the distribution of network weights by treating them as random variables. However, these methods are affected by the challenge of convergence and have a large number of computations. The dropout method has alleviated this issue to a certain extent [12]. Another uncertainty estimation way is to learn an ensemble of deep networks [14]. Recently, to alleviate computational complexity and overconfidence [25], deterministic-based methods [17, 19, 25, 26, 32] have been proposed to directly output uncertainty in a single forward pass through the network. For multimodal uncertainty estimation, the Trusted Multi-view Classification (TMC) [8] is a representative method that proposes a new paradigm of multi-view learning by dynamically integrating different views at the evidence level. However, TMC has a limited ability to detect Out-Of-Distribution (OOD) samples [11]. This attributes to TMC is particularly weak in modeling epistemic uncertainty for each single view [12]. Additionally, the fusion rule in TMC fails to account for conflicting views, making it unsuitable for safety-critical deployment [30]. To address these limitations, we propose EyeMoSt, a novel evidential fusion method that models both aleatoric and epistemic uncertainty in unimodality, while efficiently integrating different modalities from a multi-distribution fusion perspective.

In this work, we propose a novel multimodality eye disease screening method, called EyeMoSt, that conducts Fundus and OCT modality fusion in a reliable

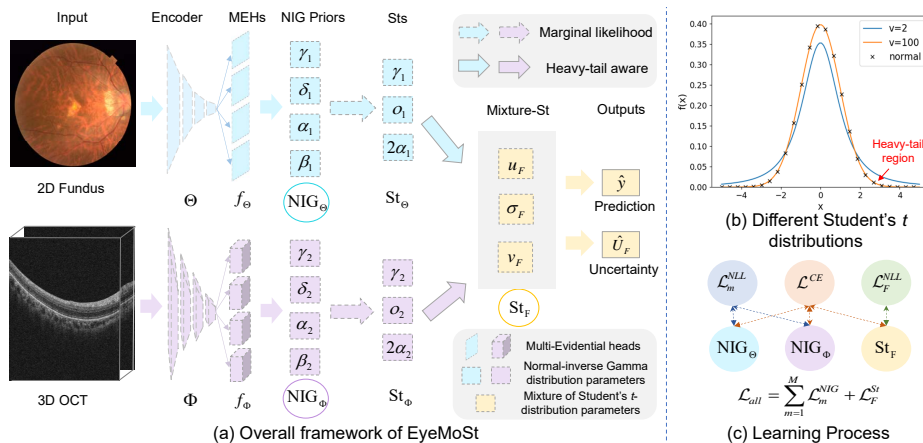


**Fig. 1.** Reliable multimodality Eye Disease Screening pipeline. (a) Overall framework of EyeMoSt. (b) Student's  $t$  Distributions with different degrees of freedom. (c) The overall learning process of EyeMoSt.

manner. Our EyeMoSt places Normal-inverse Gamma (NIG) prior distributions over the pre-trained neural networks to directly learn both aleatoric and epistemic uncertainty for unimodality. Moreover, Our EyeMoSt introduces the Mixture of Student's  $t$  (MoSt) distributions, which provide robust classification results with global uncertainty. More importantly, MoSt endows the model with robustness under heavy-tailed property awareness. We conduct sufficient experiments on two datasets for different eye diseases (*e.g.*, glaucoma grading, age-related macular degeneration, and polypoid choroidal vasculopathy) to verify the reliability and robustness of the proposed method. In summary, the key contributions are as follows:

- 1) We propose a novel multimodality eye disease screening method, EyeMoSt, which conducts reliable fusion of Fundus and OCT modalities.
- 2) Our EyeMoSt introduces the MoSt distributions, which provide robust classification results with local and global uncertainty.
- 3) We conduct extensive experiments on two datasets for different eye diseases.

## 2 Method

In this section, we introduce the overall framework of our EyeMoSt, which efficiently estimates the aleatoric and epistemic uncertainty for unimodality and adaptively integrates Fundus and OCT modalities in principle. As shown in Fig. 1 (a), we first employ the 2D/3D neural network encoders to capture different modality features. Then, we place multi-evidential heads after the trained neural networks to model the parameters of higher-order NIG distributions for uni-

Our code has been released in <https://github.com/Cocofeat/EyeMoSt>.

modality. To merge these predicted distributions, We derive the posterior predictive of the NIG distributions as Student’s  $t$  ( $St$ ) distributions. Particularly, the Mixture of Student’s  $t$  (MoSt) distributions is introduced to integrate the distributions of different modalities in principle. Finally, we elaborate on the training pipeline for the model evidence acquisition.

Given a multimodality eye dataset  $\mathcal{D} = \left\{ \left\{ \mathbf{x}_m^i \right\}_{m=1}^M \right\}$  and the corresponding label  $y^i$ , the intuitive goal is to learn a function that can classify different categories. Fundus and OCT are common imaging modalities for eye disease screening. Therefore, here  $M=2$ ,  $\mathbf{x}_1^i$  and  $\mathbf{x}_2^i$  represent Fundus and OCT input modality data, respectively. We first train 2D encoder  $\Theta$  of Res2Net [7] and 3D encoder  $\Phi$  of MedicalNet [5] to identify the feature-level informativeness, which can be defined as  $\Theta(\mathbf{x}_1^i)$  and  $\Phi(\mathbf{x}_2^i)$ , respectively.

## 2.1 Uncertainty estimation for unimodality

We extend the deep evidential regression model [1] to multimodality evidential classification for eye disease screening. To this end, to model the uncertainty for Fundus or OCT modality, we assume that the observe label  $y^i$  is drawn from a Gaussian  $\mathcal{N}(y^i|\mu, \sigma^2)$ , whose mean and variance are governed by an evidential prior named the NIG distribution:

$$\text{NIG}(\mu, \sigma^2|\mathbf{p}_m) = \mathcal{N}\left(\mu|\gamma_m, \frac{\sigma^2}{\delta_m}\right) \Gamma^{-1}(\sigma^2|\alpha_m, \beta_m), \quad (1)$$

where  $\Gamma^{-1}$  is an inverse-gamma distribution,  $\gamma_m \in \mathbb{R}, \delta_m > 0, \alpha_m > 1, \beta_m > 0$  are the learning parameters. Specifically, the multi-evidential heads will be placed after the encoders  $\Theta$  and  $\Phi$  (as shown in Fig. 1 (a)), which outputs the prior NIG parameters  $\mathbf{p}_m = (\gamma_m, \delta_m, \alpha_m, \beta_m)$ . As a result, the aleatoric (AL) and epistemic (EP) uncertainty can be estimated by the  $\mathbb{E}[\sigma^2]$  and the  $\text{Var}[\mu]$ , respectively, as:

$$\text{AL} = \mathbb{E}[\sigma^2] = \frac{\beta_m}{\alpha_m - 1}, \quad \text{EP} = \text{Var}[\mu] = \frac{\beta_m}{\delta_m(\alpha_m - 1)}. \quad (2)$$

Then, given the evidence distribution parameter  $\mathbf{p}_m$ , the marginal likelihood is calculated by marginalizing the likelihood parameter:

$$p(y^i|x_m^i, \mathbf{p}_m) = \int_{\mu} \int_{\sigma^2} p(y^i|x_m^i, \mu, \sigma^2) \text{NIG}(\mu, \sigma^2|\mathbf{p}_m) d\mu d\sigma^2. \quad (3)$$

Interacted by the prior and the Gaussian likelihood of each unimodality [1], its analytical solution does exist and yields an  $St$  prediction distribution as:

$$\begin{aligned} p(y^i|x_m^i, \mathbf{p}_m) &= \frac{\Gamma(\alpha_m + \frac{1}{2})}{\Gamma(\alpha_m)} \sqrt{\frac{\delta_m}{2\pi\beta_m(1+\delta_m)}} \left(1 + \frac{\delta_m(y^i - \gamma_m)^2}{2\beta_m(1+\delta_m)}\right)^{-(\alpha_m + \frac{1}{2})} \\ &= St(y^i; \gamma_m, o_m, 2\alpha_m), \end{aligned} \quad (4)$$

with  $o_m = \frac{\beta_m(1 + \delta_m)}{\delta_m \alpha_m}$ . The complete derivations of Eq. 4 are available in Supplementary S1.1. Thus, the two modalities distributions are transformed into the student's  $t$  Distributions  $St(y^i; u_m, \Sigma_m, v_m) = St(y^i; \gamma_m, o_m, 2\alpha_m)$ , with  $u_m \in \mathbb{R}, \Sigma_m > 0, v_m > 2$ .

## 2.2 Mixture of Student's $t$ Distributions (MoSt)

Then, we focus on fusing multiple  $St$  Distributions from different modalities. How to rationally integrate multiple  $St$ s into a unified  $St$  is the key issue. To this end, the joint modality of distribution can be denoted as:

$$St(y^i; u_F, \Sigma_F, v_F) = St\left(y^i; \begin{bmatrix} u_1^i \\ u_2^i \end{bmatrix}, \begin{bmatrix} \Sigma_{11} & \Sigma_{12} \\ \Sigma_{21} & \Sigma_{22} \end{bmatrix}, \begin{bmatrix} v_1^i \\ v_2^i \end{bmatrix}\right). \quad (5)$$

In order to preserve the closed  $St$  distribution form and the heavy-tailed properties of the fusion modality, the updated parameters are given by [24]. In simple terms, we first adjust the degrees of freedom of the two distributions to be consistent. As shown in Fig. 1 (b), the smaller values of degrees of freedom (DOF)  $v$  has heavier tails. Therefore, we construct the decision value  $\tau_m = v_m$  to approximate the parameters of the fused distribution. We assume that multiple  $St$  distributions are still an approximate  $St$  distribution after fusion. Assuming that the degrees of freedom of  $\tau_1$  are smaller than  $\tau_2$ , then, the fused  $St$  distribution  $St(y^i; u_F, \Sigma_F, v_F)$  will be updated as:

$$v_F = v_1, \quad u_F = u_1, \quad \Sigma_F = \frac{1}{2} \left( \Sigma_1 + \frac{v_2(v_1 - 2)}{v_1(v_2 - 2)} \Sigma_2 \right). \quad (6)$$

More intuitively, the above formula determines the modality with a stronger heavy-tailed attribute. That is, according to the perceived heavy-tailed attribute of each modality, the most robust modality is selected as the fusion modality. Finally, the prediction and uncertainty of the fusion modality is given by:

$$\hat{y}^i = \mathbb{E}_{p(x_F^i, \mathbf{P}_F)} [y^i] = u_F, \quad \hat{U}_F = \mathbb{E} [\sigma_F^2] = \Sigma_F \frac{v_F}{v_F - 2}. \quad (7)$$

## 2.3 Learning the evidential distributions

Under the evidential learning framework, we expect more evidence to be collected for each modality, thus, the proposed model is expected to maximize the likelihood function of the model evidence. Equivalently, the model is expected to minimize the negative log-likelihood function, which can be expressed as:

$$\begin{aligned} \mathcal{L}_m^{NLL} = & \log \frac{\Gamma(\alpha_m) \sqrt{\frac{\pi}{\delta_m}}}{\Gamma(\alpha_m + \frac{1}{2})} - \alpha_m \log(2\beta_m(1 + \delta_m)) \\ & + \left( \alpha_m + \frac{1}{2} \right) \log \left( (y^i - \gamma_m)^2 \delta_m + 2\beta_m(1 + \delta_m) \right). \end{aligned} \quad (8)$$

Then, to fit the classification tasks, we introduce the cross entropy term  $\mathcal{L}_m^{CE}$ :

$$\mathcal{L}_m^{NIG} = \mathcal{L}_m^{NLL} + \lambda \mathcal{L}_m^{CE}, \quad (9)$$

where  $\lambda$  is the balance factor set to 0.5. For further information on the selection of hyperparameter  $\lambda$ , please refer to Supplementary S2. Similarly, for the fusion modality, we first maximize the likelihood function of the model evidence as follows:

$$\mathcal{L}_F^{NLL} = \log \Sigma_F + \log \frac{\Gamma\left(\frac{v_F}{2}\right)}{\Gamma\left(\frac{v_F+1}{2}\right)} + \log \sqrt{v_F \pi} + \frac{(v_F + 1)}{2} \log \left( 1 + \frac{(y^i - u_F)^2}{v_F \Sigma_F} \right), \quad (10)$$

Complete derivations of Eq. 10 are available in Supplementary S1.2. Then, to achieve better classification performance, the cross entropy term  $\mathcal{L}_m^{CE}$  is also introduced into Eq. 10 as below:

$$\mathcal{L}_F^{St} = \mathcal{L}_F^{NLL} + \lambda \mathcal{L}_F^{CE}, \quad (11)$$

Totally, the evidential learning process for multimodality screening can be denoted as:

$$\mathcal{L}_{all} = \sum_{m=1}^M \mathcal{L}_m^{NIG} + \mathcal{L}_F^{St}. \quad (12)$$

In this paper, we mainly consider the fusion of two modalities,  $M = 2$ .

### 3 Experiments

**Datasets:** In this paper, we verify the effectiveness of EyeMoSt on the two datasets. For the glaucoma recognition, We validate the proposed method on the GAMMA [29] dataset. It contains 100 paired cases with a three-level glaucoma grading. They are divided into the training set and test set with 80 and 20 respectively. We conduct the five-fold cross-validation on it to prevent performance improvement caused by accidental factors. Then, we test our method on the in-house collected dataset, which includes Age-related macular degeneration (AMD) and polypoid choroidal vasculopathy (PCV) diseases. They are divided into training, validation, and test sets with 465, 69, and 70 cases respectively. More details of the dataset can be found in Supplementary S2. Both of these datasets are including the paired cases of Fundus (2D) and OCT (3D).

**Training Details:** Our proposed method is implemented in PyTorch and trained on NVIDIA GeForce RTX 3090. Adam optimization [13] is employed to optimize the overall parameters with an initial learning rate of 0.0001. The maximum of epoch is 100. The data augmentation techniques for GAMMA dataset are similar to [3], including random grayscaling, random color jitter, and random horizontal flipping. All inputs are uniformly adjusted to  $256 \times 256$  and  $128 \times 256 \times 128$  for Fundus and OCT modalities. The batch size is 16.

---

The ethical approval of this dataset was obtained from the Ethical Committee.

**Table 1.** Comparisons with different algorithms on the GAMMA and in-house dataset. F and O denote the Fundus and OCT modalities, respectively. The top-2 results are highlighted in Red and Blue. Higher ACC and Kappa, and Lower ECE mean better.

Methods	GAMMA dataset						In-house dataset					
	Original		Gaussian noise				Original		Gaussian noise			
			$\sigma=0.1$ (F)		$\sigma=0.3$ (O)				$\sigma=0.1$ (F)		$\sigma=0.3$ (O)	
	ACC	Kappa	ACC	Kappa	ACC	Kappa	ACC	ECE	ACC	ECE	ACC	ECE
B-IF	0.700	0.515	0.623	0.400	0.530	0.000	0.800	0.250	0.593	0.450	0.443	0.850
B-EF [10]	0.660	0.456	0.660	0.452	0.500	0.000	0.800	0.200	0.777	0.223	0.443	0.557
$M^2$ LC [28]	0.710	0.527	0.660	0.510	0.500	0.000	0.814	0.186	0.786	0.214	0.443	0.557
MCDO [6]	0.758	0.636	0.601	0.341	0.530	0.000	0.786	0.214	0.771	0.304	0.429	0.571
DE [14]	0.710	0.539	0.666	0.441	0.530	0.000	0.800	0.200	0.800	0.200	0.609	0.391
TMC [8]	0.810	0.658	0.430	0.124	0.550	0.045	0.829	0.171	0.814	0.186	0.443	0.557
Our	0.850	0.754	0.663	0.458	0.830	0.716	0.829	0.171	0.800	0.200	0.829	0.171

**Compared Methods & Metrics:** We compare the following six methods: For different fusion stage strategies, **a) B-EF** Baseline of the early fusion [10] strategy, **b) B-IF** Baseline of the intermediate typical fusion method, **c)  $M^2$ LC** [28] of the intermediate fusion method and the later fusion method **d) TMC** [8] are used as comparisons. B-EF is first integrated at the data level, and then passed through the same MedicalNet [5]. B-IF first extracts features by the encoders (same with us), and then concatenates their output features as the final prediction. For the uncertainty quantification methods, **e) MCDO** (Monte Carlo Dropout) employs the test time dropout as an approximation of a Bayesian neural network [6]. **f) DE** (Deep ensemble) quantifies the uncertainties by ensembling multiple models [14]. We adopt the accuracy (ACC) and Kappa metrics for intuitive comparison with different methods. Particularly, expected calibration error (ECE) [20] is used to compare the calibration of the uncertainty algorithms.

**Comparison and Analysis:** We reported our algorithm with different methods on the GAMMA and in-house datasets in Tab. 3. First, we compare these methods under the clean multimodality eye data. Our method obtained competitive results in terms of ACC and Kappa. Then, to verify the robustness of our model, we added Gaussian noise to Fundus or OCT modality ( $\sigma = 0.1/0.3$ ) on the two datasets. Compared with other methods, our EyeMoSt maintains classification accuracy in noisy OCT modality, while comparable in noisy Fundus modality. More generally, we added different Gaussian noises to Fundus or OCT modality, as shown in Fig. 2. The same conclusion can be drawn from Fig. 2. This is attributed to the perceived long tail in the data when fused. The visual comparisons of different noises to the Fundus/OCT modality on the in-house dataset can be found in Supplementary S2. To further quantify the reliability of uncertainty estimation, we compared different algorithms using the ECE indicator. As shown in Tab. 3 and Fig. 2, our proposed algorithm performs better in both clean and single pollution modalities. The inference times of the uncertainty-based methods on two modalities on the in-house dataset are 5.01s

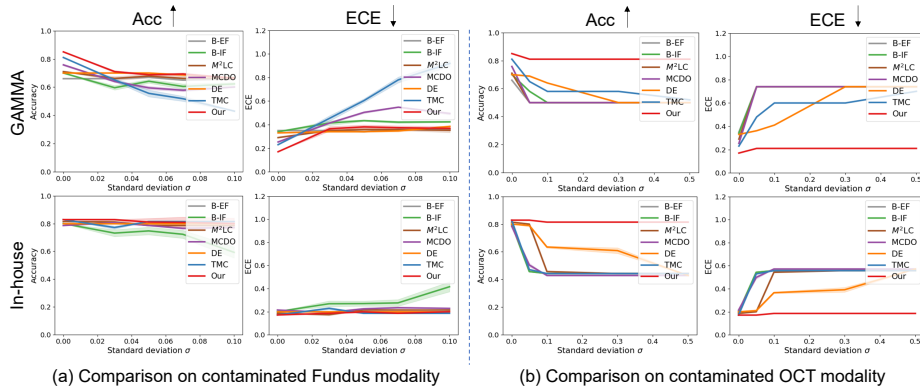


**Fig. 2.** Accuracy and ECE performance of different algorithms in contaminated single modality with different levels of noise on GAMMA and in-house datasets.

(MCDO), 8.28s (DE), 3.98s (TMC), and 3.22s (Ours). It can be concluded that the running time of EyeMoSt is lower than other methods. In brief, we conclude that our proposed model is more robust and reliable than the above methods.

#### Understanding uncertainty for unimodality/multimodality eye data:

To make progress towards the multimodality ophthalmic clinical application of uncertainty estimation, we conducted unimodality and multimodality uncertainty analysis for eye data. First, we add more Gaussian noise with varying variances to the unimodality (Fundus or OCT) in the GAMMA and in-house datasets to simulate OOD data. The original samples without noise are denoted as in-distribution (ID) data. Fig. 3 (a) shows a strong relationship between uncertainty and OOD data. Uncertainty in unimodality images increases positively with noise. Here, uncertainty acts as a tool to measure the reliable unimodality eye data. Second, we analyze the uncertainty density of unimodality and fusion modality before and after adding Gaussian noise. As shown in Fig. 3 (b), take adding noise with  $\sigma = 0.1$  to the Fundus modality on the GAMMA dataset as an example. Before the noise is added, the uncertainty distributions of unimodality and fusion modality are relatively concentrated. After adding noise, the uncertainty distribution of the fusion modality is closer to that of the modality without noise. Hence, EyeMoSt can serve as a tool for measuring the reliable modality in ophthalmic multimodality data fusion. To this end, our algorithm can be used as an out-of-distribution detector and data quality discriminator to inform reliable and robust decisions for multimodality eye disease screening.

## 4 Conclusion

In this paper, we propose the EyeMoSt for reliable and robust screening of eye diseases using evidential multimodality fusion. Our EyeMoSt produces the uncertainty for unimodality and then adaptively fuses different modalities in a distribution perspective. The different NIG evidence priors are employed to



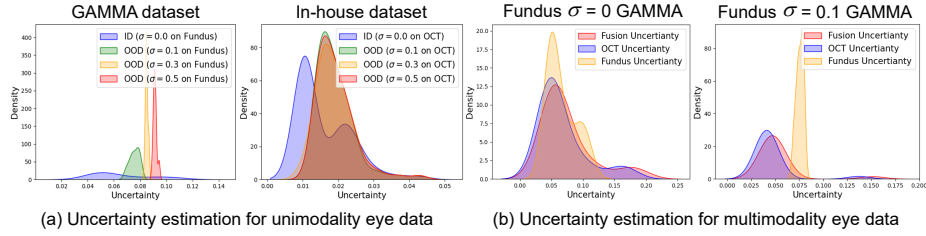


**Fig. 3.** Uncertainty density of unimodality and multimodality eye data.

model the distribution of encoder observations, which supports the backbones to directly learn aleatoric and epistemic uncertainty. We then derive an analytical solution to the Student’s  $t$  distributions of the NIG evidence priors on the Gaussian likelihood function. Furthermore, we propose the MoSt distributions in principle adaptively integrates different modalities, which endows the model with heavy-tailed properties and is more robust and reliable for eye disease screening. Extensive experiments show that the robustness and reliability of our method in classification and uncertainty estimation on GAMMA and in-house datasets are competitive with previous methods. Overall, our approach has the potential to multimodality eye data discriminator for trustworthy medical AI decision-making. In future work, our focus will be on incorporating uncertainty into the training process and exploring the application of reliable multimodality screening for eye diseases in a clinical setting.

**Acknowledgements:** This work was supported by the National Research Foundation, Singapore under its AI Singapore Programme (AISG Award No: AISG2-TC-2021-003), A\*STAR AME Programmatic Funding Scheme Under Project A20H4b0141, A\*STAR Central Research Fund, the Science and Technology Department of Sichuan Province (Grant No. 2022YFS0071 & 2023YFG0273), and the China Scholarship Council (No. 202206240082).

## References

1. Amini, A., Schwarting, W., Soleimany, A., Rus, D.: Deep evidential regression. *Advances in Neural Information Processing Systems* **33**, 14927–14937 (2020)
2. Baltrušaitis, T., Ahuja, C., Morency, L.P.: Multimodal machine learning: A survey and taxonomy. *IEEE transactions on pattern analysis and machine intelligence* **41**(2), 423–443 (2018)
3. Cai, Z., Lin, L., He, H., Tang, X.: Corolla: an efficient multi-modality fusion framework with supervised contrastive learning for glaucoma grading. In: *IEEE International Symposium on Biomedical Imaging (ISBI)*. pp. 1–4. IEEE (2022)
4. Cai, Z., Lin, L., He, H., Tang, X.: Uni4eye: Unified 2d and 3d self-supervised pre-training via masked image modeling transformer for ophthalmic image classification. In: *Medical Image Computing and Computer Assisted Intervention*. pp. 88–98. Springer (2022)
5. Chen, S., Ma, K., Zheng, Y.: Med3d: Transfer learning for 3d medical image analysis. *arXiv preprint arXiv:1904.00625* (2019)

6. Gal, Y., Ghahramani, Z.: Dropout as a bayesian approximation: Representing model uncertainty in deep learning. In: international conference on machine learning. pp. 1050–1059. PMLR (2016)
7. Gao, S.H., Cheng, M.M., Zhao, K., Zhang, X.Y., Yang, M.H., Torr, P.: Res2net: A new multi-scale backbone architecture. *IEEE Transactions on Pattern Analysis and Machine Intelligence* **43**(2), 652–662 (2021)
8. Han, Z., Zhang, C., Fu, H., Zhou, J.T.: Trusted multi-view classification. In: International Conference on Learning Representations (2020)
9. He, X., Deng, Y., Fang, L., Peng, Q.: Multi-modal retinal image classification with modality-specific attention network. *IEEE transactions on medical imaging* **40**(6), 1591–1602 (2021)
10. Hua, C.H., Kim, K., Huynh-The, T., You, J.I., Yu, S.Y., Le-Tien, T., Bae, S.H., Lee, S.: Convolutional network with twofold feature augmentation for diabetic retinopathy recognition from multi-modal images. *IEEE Journal of Biomedical and Health Informatics* **25**(7), 2686–2697 (2020)
11. Jung, M.C., Zhao, H., Dipnall, J., Gabbe, B., Du, L.: Uncertainty estimation for multi-view data: The power of seeing the whole picture. In: Advances in Neural Information Processing Systems (2022)
12. Kendall, A., Gal, Y.: What uncertainties do we need in bayesian deep learning for computer vision? In: Advances in Neural Information Processing Systems (2017)
13. Kingma, D., Ba, J.: Adam: A method for stochastic optimization. *Computer Science* (2014)
14. Lakshminarayanan, B., Pritzel, A., Blundell, C.: Simple and scalable predictive uncertainty estimation using deep ensembles. *Advances in Neural Information Processing Systems* **30** (2017)
15. Li, X., Jia, M., Islam, M.T., Yu, L., Xing, L.: Self-supervised feature learning via exploiting multi-modal data for retinal disease diagnosis. *IEEE Transactions on Medical Imaging* **39**(12), 4023–4033 (2020)
16. Li, Y., El Habib Daho, M., Conze, P.H., et al.: Multimodal information fusion for glaucoma and diabetic retinopathy classification. In: Ophthalmic Medical Image Analysis Workshop with MICCAI. pp. 53–62. Springer (2022)
17. Liu, J.Z., Lin, Z., Padhy, S., Tran, D., Bedrax-Weiss, T., Lakshminarayanan, B.: Simple and principled uncertainty estimation with deterministic deep learning via distance awareness. In: Proceedings of the 34th International Conference on Neural Information Processing Systems (2020)
18. MacKay, D.J.: A practical bayesian framework for backpropagation networks. *Neural computation* **4**(3), 448–472 (1992)
19. Malinin, A., Gales, M.: Predictive uncertainty estimation via prior networks. *Advances in neural information processing systems* **31** (2018)
20. Maronas, J., Paredes, R., Ramos, D.: Calibration of deep probabilistic models with decoupled bayesian neural networks. *Neurocomputing* **407**, 194–205 (2020)
21. Neal, R.M.: Bayesian learning for neural networks, vol. 118. Springer Science & Business Media (2012)
22. Ranganath, R., Gerrish, S., Blei, D.: Black box variational inference. In: Artificial intelligence and statistics. pp. 814–822. PMLR (2014)
23. Rodrigues, E.O., Conci, A., Liatsis, P.: Element: Multi-modal retinal vessel segmentation based on a coupled region growing and machine learning approach. *IEEE Journal of Biomedical and Health Informatics* **24**(12), 3507–3519 (2020)
24. Roth, M., Özkan, E., Gustafsson, F.: A student’s t filter for heavy tailed process and measurement noise. In: 2013 IEEE International Conference on Acoustics, Speech and Signal Processing. pp. 5770–5774. IEEE (2013)

25. Sensoy, M., Kaplan, L., Kandemir, M.: Evidential deep learning to quantify classification uncertainty. In: Proceedings of the 32nd International Conference on Neural Information Processing Systems. pp. 3183–3193 (2018)
26. Van Amersfoort, J., Smith, L., Teh, Y.W., Gal, Y.: Uncertainty estimation using a single deep deterministic neural network. In: International Conference on Machine Learning. pp. 9690–9700. PMLR (2020)
27. Wang, W., Li, X., Xu, Z., Yu, W., Zhao, J., Ding, D., Chen, Y.: Learning two-stream cnn for multi-modal age-related macular degeneration categorization. *IEEE Journal of Biomedical and Health Informatics* **26**(8), 4111–4122 (2022)
28. Woo, S., Park, J., Lee, J.Y., Kweon, I.S.: Cbam: Convolutional block attention module. In: Proceedings of the European conference on computer vision (ECCV). pp. 3–19 (2018)
29. Wu, J., Fang, H., Li, F., et al.: Gamma challenge: glaucoma grading from multi-modality images. arXiv preprint arXiv:2202.06511 (2022)
30. Zadeh, L.A.: Review of a mathematical theory of evidence. *AI magazine* **5**(3), 81–81 (1984)
31. Zhou, T., Ruan, S., Canu, S.: A review: Deep learning for medical image segmentation using multi-modality fusion. *Array* **3**, 100004 (2019)
32. Zou, K., Yuan, X., Shen, X., Chen, Y., Wang, M., Goh, R.S.M., Liu, Y., Fu, H.: Evidencecap: Towards trustworthy medical image segmentation via evidential identity cap. arXiv preprint arXiv:2301.00349 (2023)

## Supplementary Materials

### 1. Derivations

#### 1.1. Decomposition details of Eq. 4

In this subsection, a Student-t predictive distribution is generated by deriving the posterior predictor from a NIG distribution:

$$\begin{aligned}
p(y^i | x_m^i, \mathbf{p}_m) &= \int_{\mu} \int_{\sigma^2} p(y^i | x_m^i, \mu, \sigma^2) \text{NIG}(\mu, \sigma^2 | \mathbf{p}_m) d\mu d\sigma^2 \\
&= \int_{\mu} \int_{\sigma^2} \left[ \sqrt{\frac{1}{2\pi\sigma^2}} e^{-\frac{(y^i - \mu)^2}{2\sigma^2}} \right] \left[ \frac{\beta_m^\alpha \sqrt{\delta_m}}{\Gamma(\alpha_m) \sqrt{2\pi\sigma^2}} \left(\frac{1}{\sigma^2}\right)^{\alpha_m+1} e^{-\frac{2\beta_m + \delta_m(\gamma_m - \mu)^2}{2\sigma^2}} \right] d\mu d\sigma^2 \\
&= \int_{\sigma^2} \frac{\beta_m^\alpha \sigma^{-2\alpha_m - 3}}{\sqrt{2\pi(1+1/\delta_m)} \Gamma(\alpha_m)} e^{-\frac{2\beta_m + \frac{\delta_m(y^i - \gamma_m)^2}{2\sigma^2}}{\delta_m + 1}} d\sigma^2 \\
&= \frac{\Gamma(\alpha_m + \frac{1}{2})}{\Gamma(\alpha_m)} \sqrt{\frac{\delta_m}{2\pi\beta_m(1+\delta_m)}} \left(1 + \frac{\delta_m(y^i - \gamma_m)^2}{2\beta_m(1+\delta_m)}\right)^{-(\alpha_m + \frac{1}{2})} \\
&= \text{St}(y^i; \gamma_m, 0_m, 2\alpha_m)
\end{aligned} \tag{S1}$$

#### 1.2. Decomposition details of Eq. 10

For the fusion modality, we expect more evidence to be collected, which is maximizing the likelihood function of the Student's  $t$ . Equivalently, we minimize the negative log-likelihood function, which can be expressed as:

$$p(y^i; u_F, \Sigma_F; v_F) = -\log \left( \frac{\Gamma(\frac{v_F+1}{2})}{\Sigma_F \Gamma(\frac{v_F}{2}) \sqrt{v_F \pi}} \left(1 + \frac{(y^i - u_F)^2}{v_F \Sigma_F}\right)^{-\frac{1}{2}(v_F+1)} \right), \tag{S2}$$

Therefore, we train the model to minimize the above equation by:

$$\begin{aligned}
\mathcal{L}_F^{NLL} &= \log \Sigma_F + \log \frac{\Gamma(\frac{v_F}{2})}{\Gamma(\frac{v_F+1}{2})} + \log \sqrt{v_F \pi} - \log \left(1 + \frac{(y^i - u_F)^2}{v_F \Sigma_F}\right)^{-\frac{1}{2}(v_F+1)} \\
&= \log \Sigma_F + \log \frac{\Gamma(\frac{v_F}{2})}{\Gamma(\frac{v_F+1}{2})} + \log \sqrt{v_F \pi} + \frac{1}{2} (v_F + 1) \log \left(1 + \frac{(y^i - u_F)^2}{v_F \Sigma_F}\right).
\end{aligned} \tag{S3}$$

## 2. Experimental details

**Ablation study.** 1)  $\lambda$  is the balance factor between the  $\mathcal{L}_m^{NLL}$  loss and the  $\mathcal{L}_m^{CE}$  loss. In the experiments below, we demonstrate the importance of augmenting training objective with the evidence classifier loss  $\mathcal{L}_m^{CE}$  introduced in EyeMoSt.  $\lambda \in [0, 1]$  represents the importance of  $\mathcal{L}_m^{CE}$  loss. We performed parameter validation on the in-house dataset. As shown in the Tab. S1, the performance is improved after introducing  $\mathcal{L}_m^{CE}$  loss, and the best value is 0.5. 2) Ablation study for overall learning process. Further, we conduct ablation experiments on Eq. 12, as depicted in Tab. S2. Where B is the baseline of the intermediate typical fusion method. B-IF first extracts features by the encoders (same with us), and then concatenates their output features as the final prediction.  $\mathcal{L}_m^{NIG}$  represents pairwise fusion directly after establishing multi-NIG distributions.

**Table S1.** Parameter selection of  $\lambda$  on the in-house dataset

$\lambda =$	0	0.1	0.2	0.5	0.7	1.0
Acc	0.800	0.771	0.814	<b>0.829</b>	0.814	0.786
AUC	0.843	0.754	0.797	<b>0.850</b>	0.850	0.810
F1	0.794	0.762	0.808	<b>0.822</b>	0.808	0.781
Recall	0.800	0.771	0.814	<b>0.829</b>	0.814	0.786

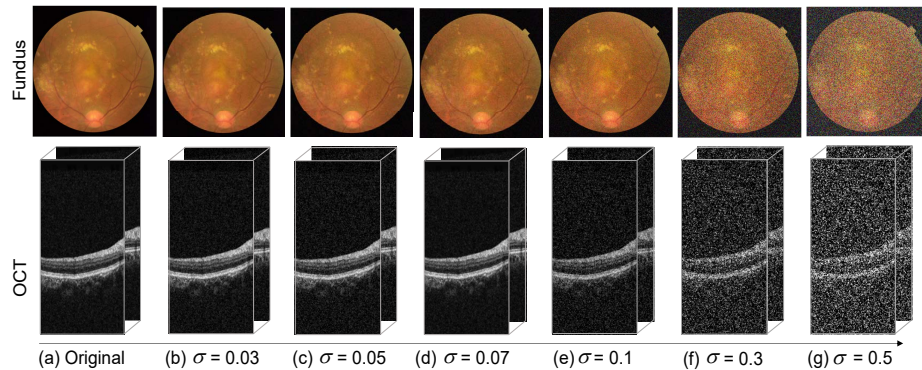
**Details of in-house dataset.** In-house dataset consists of the 265 AMD samples and 341 PCV samples. The training set, validation set, and test set include pairs of Fundus and OCT of 465, 69, and 70, respectively. The Table S3 summarizes the detailed information. The original image size of each Fundus is  $2100 \times 2000$ . We adjust it to  $256 \times 256$ . The original image size of each OCT is  $512 \times 885$ . Each eye case has 128 slices, so the 3D OCT size is adjusted to  $128 \times 256 \times 128$ . As shown in Fig. S1, we show some cases with different noise conditions.

**Table S2.** The result of ablation Study.

B	$\mathcal{L}_m^{NIG}$	$\mathcal{L}_F^{St}$	Acc	AUC	F1	Recall
✓			0.800	0.854	0.792	0.800
✓	✓		0.814	0.841	0.808	0.814
✓	✓	✓	0.829	0.850	0.822	0.829

**Table S3.** Information of in-house dataset.

In-house	Train	Validation	Test	Total
AMD	205	27	31	265
PCV	260	42	39	341
All	465	69	70	604

**Fig. S1.** Demonstration of different noise to the Fundus/OCT images on the in-house dataset.